Tunable Metallicity of the $La_{5/8}Ca_{3/8}MnO_3(001)$ Surface by an Oxygen Overlayer

K. Fuchigami,[1,2,3] Z. Gai,[1] T. Z. Ward,[1,2] L. F. Yin,[1] P. C. Snijders,[1] E. W. Plummer,[2,4] and J. Shen[1,2,*]

[1]*Materials Sciences and Technology Division, Oak Ridge National Laboratory, Oak Ridge, Tennessee 37831, USA*
[2]*Department of Physics and Astronomy, The University of Tennessee, Knoxville, Tennessee 37996, USA*
[3]*Research Laboratory, IHI Corporation, Yokohama, Kanagawa 235-8501, Japan*
[4]*Department of Physics and Astronomy, Louisiana State University, Baton Rouge, Louisiana 70803, USA*
(Received 10 November 2008; published 13 February 2009)

We studied the surface structure of $La_{5/8}Ca_{3/8}MnO_3(001)$ thin films using *in situ* scanning tunneling microscopy (STM). Atomically resolved STM images reveal that a $(\sqrt{2} \times \sqrt{2})R45^\circ$ reconstructed surface and a (1×1) surface can be converted back and forth through adsorption and desorption of oxygen at the surface. The electrical properties of the surfaces are investigated by scanning tunneling spectroscopy. $I - V$ curves clearly show that the presence of an oxygen overlayer renders the surface insulating while the (1×1) surface without the oxygen overlayer is metallic.

DOI: 10.1103/PhysRevLett.102.066104 PACS numbers: 68.37.Ef, 61.05.−a, 71.30.+h, 73.20.−r

Perovskite manganites are complex systems in which the structural, electronic, and magnetic properties are strongly coupled though not necessarily linearly [1]. A small change in one property (e.g., structure) can produce a large change in another property (e.g., the electronic state). Conceptually, creating a surface by cleaving a single crystal or growing a thin film is a controlled way to disturb the coupled system by breaking the symmetry without changing the stoichiometry. This provides the opportunity to study how structural, electronic, and magnetic properties react to the broken symmetry which may lead to completely new physical properties. For instance, a recent work reported that the surface of $La_{2-2x}Sr_{1+2x}Mn_2O_7$ is a nonmagnetic insulator despite the bulk compound being a ferromagnetic metal [2]. This naturally assembled surface insulator atop a ferromagnetic metal provides an ideal system for magnetic tunnel junction applications.

The emerging surface electronic phases can be further enriched by surface reconstructions which often occur due to bond breaking at the surface. It is of particular interest to investigate the manganites with the 113-perovskite structure whose surfaces cannot be created by cleaving but can be prepared by laser molecular beam epitaxy (laser MBE) [3]. In this Letter, we report the surface reconstructions and the corresponding electronic states of $La_{1-x}Ca_xMnO_3(001)(x = 3/8)$, which is one of the most investigated manganite systems. A reversible transition between a (1×1) and a $(\sqrt{2} \times \sqrt{2})R45^\circ$ reconstruction was observed by scanning tunneling microscopy with atomic resolution at room temperature. We provide direct experimental evidence to show that oxygen adsorption and desorption are the physical origin of this reversible structural transition. Strikingly, the (1×1) surface is metallic despite the bulk compound of $La_{5/8}Ca_{3/8}MnO_3$ being an insulator at room temperature. The $(\sqrt{2} \times \sqrt{2})R45^\circ$ surface, in contrast, is an insulator with a band gap of 1.35 eV.

We obtained the (001)-oriented surface of $La_{5/8}Ca_{3/8}MnO_3$ by growing epitaxial thin films on Nb-doped $SrTiO_3$ single crystal substrates using laser MBE. Prior to growth, the substrates were chemically etched by buffered HF followed by an *in situ* annealing at 820 °C for 30 min to ensure a TiO_2 terminated surface [4]. The growth was carried out in an ultrahigh vacuum system with a base pressure of 3×10^{-10} Torr. During growth, the substrate was kept at about 820 °C in a flowing oxygen (8% ozone) environment under a pressure of 7×10^{-4} Torr. Differentially pumped reflection high energy electron diffraction (RHEED) was used to monitor the growth quality. The film stoichiometry and quality were further examined by *ex situ* magnetic and transport measurements, which both give a T_c (260 K) that is about the same as that of the bulk (267 K). After growth, under the same oxygen pressure as during growth, samples with film thickness of 120 nm were annealed *in situ* in the growth chamber at 820 °C for a set amount of time and then allowed to cool. Annealing with an oxygen pressure that is too low $(1 \times 10^{-5}$ Torr) or too high $(1 \times 10^{-2}$ Torr) leads to various types of defects

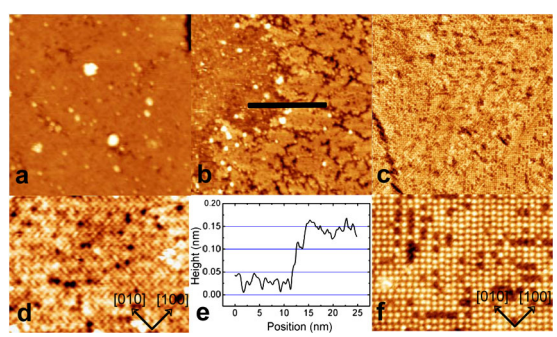

FIG. 1 (color online). STM images of $La_{5/8}Ca_{3/8}MnO_3(001)$ surfaces with a post annealing time of (a) 0 min, (b) 10 min, and (c) 30 min. The (d) and (f) are the high resolution zoom-in images of (a) and (c), which show clearly the (1×1) and the $(\sqrt{2} \times \sqrt{2})R45^\circ$ lattices, respectively. (e) is the line profile of the white mark in (b), showing the height difference of 1.3 Å of the two domains. The image areas are 60 nm × 60 nm for (a), (b), and (c), and 16 nm × 12 nm for (d) and (f).

at the surface. After evacuating the oxygen from the growth chamber, the samples were transferred *in situ* to a scanning tunneling microscope chamber with a base pressure of 1×10^{-10} Torr. All the STM images were acquired at a pressure of 1×10^{-10} Torr using mechanically cut Pt-Ir tips. A bias voltage was applied to the tip and the sample was grounded. This configuration reveals occupied or unoccupied states with the application of a positive or a negative bias, respectively.

The surface structure of LCMO films depends strongly on the time of post annealing in oxygen. Figure 1 shows STM images of LCMO surfaces with a post annealing time of (a) 0 min, (b) 10 min, and (c) 30 min. For the as-grown film without post annealing in oxygen [Fig. 1(a)], the surface has a (1×1) lattice pattern [5]. When the post annealing time is 10 min, new domains with $(\sqrt{2} \times \sqrt{2})R45°$ structures start to develop in the (1×1) structured surface [Fig. 1(b)] and coexist with the (1×1) domains. The $(\sqrt{2} \times \sqrt{2})R45°$ domains, however, have many structural defects. The marked line profile shows that the height difference between the $(\sqrt{2} \times \sqrt{2})R45°$ domains and the (1×1) domains is about 1.3 Å [Fig. 1(e)]. When the film was post annealed for 30 minutes, the surface exhibited a well-ordered $(\sqrt{2} \times \sqrt{2})R45°$ reconstruction [Fig. 1(c)], which can be seen clearly in the magnified image [Fig. 1(d)].

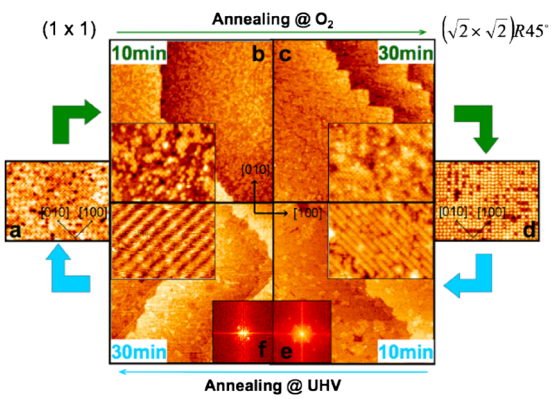

FIG. 2 (color online). Flowchart of the structure evolution between (1×1) and $(\sqrt{2} \times \sqrt{2})R45°$. Arrows indicate the conversion from annealing in oxygen (green, print in black) or UHV (blue, print in gray), respectively. Annealing the sample with the (1×1) structure (a) in oxygen at 820 °C for 10 min (b) and 30 min (c), coexist with the (1×1) structure, more and more $(\sqrt{2} \times \sqrt{2})R45°$ patches show up, and finally a full $(\sqrt{2} \times \sqrt{2})R45°$ structure (d) forms. Annealing the sample with the $(\sqrt{2} \times \sqrt{2})R45°$ structure (d) in UHV at 400 °C for 10 min (e) and 30 min (f), $(\sqrt{2} \times 2\sqrt{2})R45°$ [insert in (e)] and $(\sqrt{2} \times 3\sqrt{2})R45°$ [inset in (f)] patches show up, and finally a full (1×1) structure (a) forms. (b), (c), (e), and (f) are 150 nm × 150 nm, (a), (d) and all the high resolution insets are 16 nm × 12 nm. The fast Fourier Transform (FFT) of the STM images with $(\sqrt{2} \times 2\sqrt{2})R45°$ and $(\sqrt{2} \times 3\sqrt{2})R45°$ structures are also shown as additional insets in (e) and (f).

The (1×1) structure and the $(\sqrt{2} \times \sqrt{2})R45°$ structures can be converted back and forth through the control of adsorption and desorption of oxygen at the surface. As indicated by the green arrows (print in black) in Fig. 2, with increasing annealing time in oxygen at 820 °C, more and more $(\sqrt{2} \times \sqrt{2})R45°$ patches appear on the otherwise (1×1) surface. Over a long enough time, these patches grow until the surface has a nearly complete $(\sqrt{2} \times \sqrt{2})R45°$ structure. It is then possible to return the surface to its (1×1) structure by annealing in ultrahigh vacuum which forces oxygen desorption. As indicated by the blue arrows (print in gray) in Fig. 2, with increased annealing time at 400 °C, the $(\sqrt{2} \times \sqrt{2})R45°$ surface reduces first to reconstructions with a longer periodicity. The atomically resolved STM images reveal that the surface in Fig. 2(e) has a $(\sqrt{2} \times 2\sqrt{2})R45°$ structure, as confirmed by the fast Fourier transformation (FFT) inset. The surface in Fig. 2(f) appears to have a $(\sqrt{2} \times 3\sqrt{2})R45°$ structure. The periodicity corresponding to that of $3\sqrt{2}$ can be clearly seen in the FFT inset. Although the atomic positions along the reconstruction rows cannot be clearly distinguished because of the limited image resolution, the structural symmetry implies that the periodicity along the directions of the rows corresponds to that of $\sqrt{2}$ or longer. After a sufficient time of annealing, the surface eventually becomes the (1×1) structure. The sequential formation of $(\sqrt{2} \times \sqrt{2})R45°$, $(\sqrt{2} \times 2\sqrt{2})R45°$, and $(\sqrt{2} \times 3\sqrt{2})R45°$ upon oxygen desorption strongly hints that these surface reconstructions are associated with increasing oxygen deficiency at the surface. The $(\sqrt{2} \times 2\sqrt{2})R45°$ and the $(\sqrt{2} \times 3\sqrt{2})R45°$

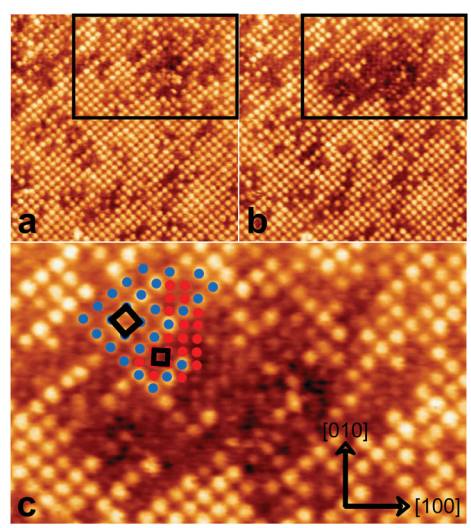

FIG. 3 (color). STM images of the LCMO surface before (a), and after (b), a STM tip scratching as described in the text (18 nm × 18 nm). (c) is the zoom in (13 nm × 8 nm) of (b). The blue dots show the $(\sqrt{2} \times \sqrt{2})R45°$ lattice, while the red dots indicate the (1×1) lattice; both unit cells are marked with black squares.

reconstructions do not appear during the oxygen adsorption process, indicating that these structures are metastable.

More direct evidence to show that the nature of the $(\sqrt{2}\times\sqrt{2})R45°$ surface is caused by an oxygen overlayer atop the (1×1) surface is given by using the STM tip to gently scratch the $(\sqrt{2}\times\sqrt{2})R45°$ surface. As shown in Fig. 3, while scanning the STM tip across a $(\sqrt{2}\times\sqrt{2})R45°$ surface [Fig. 3(a)] using a higher tunneling current of 75 pA as compared with the usual parameter of 35 pA, the tip accidentally scrapes off the $(\sqrt{2}\times\sqrt{2})R45°$ layer and exposes a new surface [Fig. 3(b)]. In the exposed surface zoomed in Fig. 3(c), the (1×1) structure (indicated by the red dots) is clearly visible in contrast to the surrounding $(\sqrt{2}\times\sqrt{2})R45°$ lattice (indicated by the blue dots). The height difference between the $(\sqrt{2}\times\sqrt{2})R45°$ surface and the exposed (1×1) patch is about 1.4 Å, which is consistent with the height of an oxygen overlayer on the (1×1) surface (Fig. 1).

Given the fact that the $SrTiO_3$ surface is terminated by a TiO_2 plane, the (1×1) surface reflects the MnO_2 terminated surface. This is because the LCMO film grows unit cell by unit cell as evidenced by RHEED oscillations as well as STM step height measurements at the initial stage of growth (not shown here) [6]. When oxygen atoms adsorb atop the MnO_2 terminated surface, the MnO_6 octahedron is completed just like that of the bulk structure. There are two possible structural models for the adsorbed oxygen atoms to generate the observed $(\sqrt{2}\times\sqrt{2})R45°$ reconstruction. In the first model, the oxygen atoms locate atop every MnO_6 octahedron. In bulk, the MnO_6 octahedra are known to tilt due to the Jahn-Teller distortion [7,8] which results in a natural $(\sqrt{2}\times\sqrt{2})R45°$ reconstruction at the surface. In the second model, the oxygen atoms sit atop every other MnO_6 octahedron and form the $(\sqrt{2}\times\sqrt{2})R45°$ lattice arrangement. The major difference between the two models is that half of the oxygen atoms are missing in the second model. Based on our observations of the structural evolution of $(\sqrt{2}\times\sqrt{2})R45° \rightarrow (\sqrt{2}\times2\sqrt{2})R45° \rightarrow (\sqrt{2}\times3\sqrt{2})R45°$ during the oxygen desorption process, we can rule out the first model because it is highly unlikely that the octahedron tilt can result in an ordering with a larger unit cell than $(\sqrt{2}\times\sqrt{2})R45°$. We thus conclude that the second structural model, i.e., the missing oxygen model (Fig. 4), explains the observed structural evolution. In fact, the second structural model with only half a monolayer of oxygen atoms is energetically favored because an increase in the number of surface oxygen atoms to a full monolayer would increase the Coulomb energy contribution to the surface total energy because of the larger amount of charge at the surface.

Remarkably, there is a dramatic difference in metallicity for the $(\sqrt{2}\times\sqrt{2})R45°$ structure and the (1×1) structure. As shown in Fig. 5, the scanning tunneling spectroscopy I/V curves (in logarithmic scale) of the $(\sqrt{2}\times\sqrt{2})R45°$ and the (1×1) surfaces are distinctly different near the Fermi energy. The $(\sqrt{2}\times\sqrt{2})R45°$ surface yields an insulating characteristic with a band gap of about 1.35 eV while the (1×1) surface is metallic and shows no band gap. The 1.35 eV gap for the $(\sqrt{2}\times\sqrt{2})R45°$ surface is comparable to the ~1 eV gap measured in the bulk [9]. We note that a similar change of metallicity has also been observed in films with a much smaller thickness (1.5 nm).

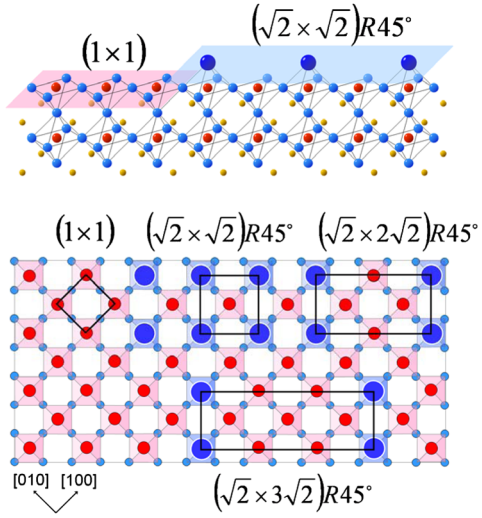

FIG. 4 (color online). Side view (upper panel) and top view (lower panel) of the stick and ball models for (1×1) and $(\sqrt{2}\times\sqrt{2})R45°$ structures, with red (print in small black), large blue (print in large black), and small blue (print in small gray) balls representing Mn, O atoms located atop the MnO_6 octahedra, and O at the MnO_6 layer, respectively. The unit cells of (1×1), $(\sqrt{2}\times\sqrt{2})R45°$, $(\sqrt{2}\times2\sqrt{2})R45°$, and $(\sqrt{2}\times3\sqrt{2})R45°$ are outlined in the lower panel.

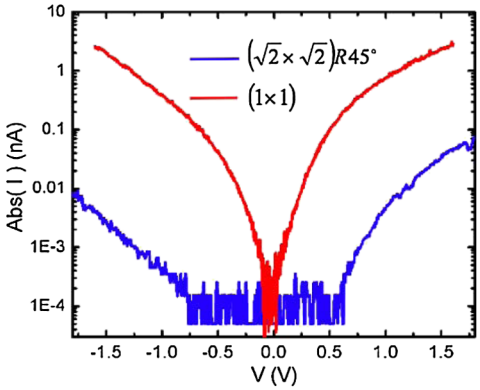

FIG. 5 (color online). Scanning tunneling spectroscopy I/V curves (shown in logarithmic scale) obtained at set points of 1.8 V/30 pA and 0.6 V/200 pA from the $(\sqrt{2}\times\sqrt{2})R45°$ and the (1×1) surfaces, respectively. The (1×1) surface shows no band gap while the $(\sqrt{2}\times\sqrt{2})R45°$ surface shows a 1.35 eV band gap. Note that the band gap for the $(\sqrt{2}\times\sqrt{2})R45°$ is intrinsic because it remains unchanged when the tip is placed further from the surface at different set points.

The insulating behavior of the $(\sqrt{2}\times\sqrt{2})R45°$ surface can be understood based on the bulk phase diagram of the LCMO material. In bulk, LCMO is a paramagnetic insulator above T_c (~267 K). Although the physical origin of the insulating behavior above T_c is not completely understood, theoretical [10] and experimental [11–13] evidence have shown that dynamic and static Jahn-Teller distortions at and above T_c play a major role in causing localization of charge carriers and thus stabilize the insulating phase. If the surface is terminated by the (La,Ca)O-plane, it should exhibit the insulating behavior from the bulk when at room temperature (well above T_c). The $(\sqrt{2}\times\sqrt{2})R45°$ surface resembles the (La,Ca)O-terminated surface in the sense that the Mn atoms are bonded with oxygen atoms to complete the MnO_6 octahedron. Missing the (La,Ca) cations in the $(\sqrt{2}\times\sqrt{2})R45°$ surface may not change the local density of states (DOS) of the MnO_2 layer because the cations do not contribute to bonding and the cation-derived DOS is located far from the Fermi level. Their only contribution is in donating their valence electrons to the Mn and O bands. Therefore, it is not surprising that the $(\sqrt{2}\times\sqrt{2})R45°$ surface also exhibits the insulating behavior from the bulk.

For the MnO_2 terminated (1×1) surface, the $e_{g(3z^2-r^2)}$ orbital is expected to have a lower binding energy than the $e_{g(x^2-y^2)}$ orbitals due to a lack of Coulomb repulsion from the p_z electron of the missing oxygen at the top of the octahedron [14]. Compared with the $e_{g(x^2-y^2)}$, orbital, the $e_{g(3z^2-r^2)}$ orbital is more delocalized around the Mn ionic core, leading to more overlapping with the p orbital of the neighboring oxygen atoms. In this regard, the $e_{g(3z^2-r^2)}$ orbital derived band has a larger width than that derived from the $e_{g(x^2-y^2)}$ orbital. Moreover, theoretical calculations of the MnO_2 terminated surface, while being inconsistent in whether the magnetic order is ferromagnetic [13,15,16] or antiferromagnetic [17], all conclude that $e_{g(3z^2-r^2)}$ is the dominant state for the MnO_2 terminated surface. This gives rise to a conductive characteristic along the orbital direction (z; normal to the surface). With these theoretical results, it can be assumed that the MnO_2 termination provides larger surface conductivity than the (La, Ca)O termination. However, a full understanding of this issue will rely on a theoretical calculation of the electronic structure of the (1×1) surface for the LCMO thin film.

In summary, we have identified two stable surface structures on the $La_{5/8}Ca_{3/8}MnO_3(001)$ surface, $(\sqrt{2}\times\sqrt{2})R45°$ and (1×1), which are, respectively, insulating and metallic. The $(\sqrt{2}\times\sqrt{2})R45°$ structure likely reflects the fact that only half of the MnO_6 octahedra are completed by oxygen adatoms. This argument is strengthened by the fact that the $(\sqrt{2}\times\sqrt{2})R45°$ surface structure can be converted into the (1×1) structure when the oxygen atoms are desorbed from the surface. The observed metallic behavior of the (1×1) surface indicates that the broken symmetry at the surface can have a dramatic impact on the physical properties of the manganites systems, offering a new pathway to study emerging phenomena in complex systems.

The authors would like to thank Zhong Fang for valuable discussions. This effort was supported in part by the Division of Materials Science and Engineering, U.S. DOE, under contract with UT-Battelle, LLC, DE-AC05-00O822725. K. F. and E. W. P. have received support from NSF and DOE (DMS and E) (NSF-DMR-0451163).

*To whom correspondence should be addressed.

[1] E. Dagotto, T. Hotta, and A. Moreo, Phys. Rep. **344**, 1 (2001).
[2] J. W. Freeland *et al.*, Nature Mater. **4**, 62 (2005).
[3] J. X. Ma, D. T. Gillaspie, E. W. Plummer, and J. Shen, Phys. Rev. Lett. **95**, 237210 (2005).
[4] M. Kawasaki *et al.*, Science **266**, 1540 (1994).
[5] The (1×1) pattern is, in fact, not a true (1×1) in the sense that different atomic sites exhibit different contrast. This is likely caused by the presence of Mn^{3+} and Mn^{4+} ions. We still name such a structure as (1×1) with an understanding that the true translational symmetry does not exist due to the Ca doping.
[6] To prove the surface is terminated with a MnO_2 plane, we have grown a film of 0.4 monolayer thickness. The STM height measurements show all islands have a step height of 0.4 nm, which shows that the unit cell by unit cell growth starts from the very beginning. This implies that the surfaces of the LCMO films are terminated with a MnO_2 plane, which is consistent with our earlier observation in Ref. [3].
[7] P. Dai *et al.*, Phys. Rev. B **54**, R3694 (1996).
[8] P. G. Radaelli *et al.*, Phys. Rev. B **56**, 8265 (1997).
[9] J. Y. T. Weil, N.-C. Yehl, and R. P. Vasquez, Phys. Rev. Lett. **79**, 5150 (1997).
[10] A. J. Millis, Phys. Rev. B **53**, 8434 (1996); A. J. Millis, Nature (London) **392**, 147 (1998); A. J. Millis, R. Mueller, and B. I. Shraiman, Phys. Rev. B **54**, 5389 (1996).
[11] M. Ziese and C. Srinitiwarawong, Phys. Rev. B **58**, 11519 (1998).
[12] C. P. Adams *et al.*, Phys. Rev. Lett. **85**, 3954 (2000).
[13] M. Quijada *et al.*, Phys. Rev. B **58**, 16093 (1998).
[14] H. Zenia, G. A. Gehring, G. Banach, and W. M. Temmerman, Phys. Rev. B **71**, 024416 (2005).
[15] M. J. Calderon, L. Brey, and F. Guinea, Phys. Rev. B **60**, 6698 (1999).
[16] A. Filippetti and W. E. Pickett, Phys. Rev. B **62**, 11571 (2000).
[17] Z. Fang and K. Terakura, J. Phys. Soc. Jpn. **70**, 3356 (2001).